

Exact Results for Evaporating Black Holes in
Curvature-Squared Lovelock Gravity :
Gauss-Bonnet Greybody Factors

J. Grain,¹ A. Barrau¹ and P. Kanti²

¹ Laboratory for Subatomic Physics and Cosmology,
Joseph Fourier University, CNRS-IN 2P 3,
53, avenue des Martyres, 38026 Grenoble cedex, France

² Department of Mathematical Sciences, University of Durham,
Science Site, South Road, Durham DH1 3LE, United Kingdom

Abstract

Lovelock gravity is an important extension of General Relativity that provides a promising framework to study curvature corrections to the Einstein action, while avoiding ghosts and keeping second order field equations. This paper derives the greybody factors for D -dimensional black holes arising in a theory with a Gauss-Bonnet curvature-squared term. These factors describe the non-trivial coupling between black holes and quantum fields during the evaporation process: they can be used both from a theoretical viewpoint to investigate the intricate spacetime structure around such a black hole, and for phenomenological purposes in the framework of braneworld models with a low Planck scale. We derive exact spectra for the emission of scalar, fermion and gauge fields emitted on the brane, and for scalar fields emitted in the bulk, and demonstrate how the Gauss-Bonnet term can change the bulk-to-brane emission rates ratio in favour of the bulk channel in particular frequency regimes.

PACS Numbers: 04.70.Dy, 04.50.+h

1 Introduction

In any attempt to perturbatively quantize gravity as a field theory, higher-derivative interactions must be included in the action. Such terms also arise in the effective low-energy action of string theories. Furthermore, it has been argued that higher-derivative gravity theories are intrinsically attractive as in many cases they display features of renormalizability and asymptotic freedom. Among such approaches, Lovelock gravity [1] is especially interesting as the resulting equations of motion contain no more than second derivatives of the metric, and as they are free of ghosts when expanding around flat space. Among the dimensionally extended Euler densities used in the Lovelock Lagrangian, it is reasonable to consider that the four-derivative Gauss-Bonnet term is the dominant correction to the Einstein-Hilbert action [2]. The action therefore reads as:

$$S_{GB} = \frac{1}{16G} \int d^D x \sqrt{-g} \left(R + \alpha (R^2 - 4R_{\mu\nu}R^{\mu\nu} + R_{\mu\nu\rho\sigma}R^{\mu\nu\rho\sigma}) \right);$$

where α is a coupling constant of dimension $(\text{length})^2$, and G the D -dimensional Newton's constant defined as $G = 1/M^{D-2}$ in terms of the fundamental Planck scale M . In four dimensions, the Gauss-Bonnet term is a total derivative, but it becomes dynamical for $D > 4$. The thermodynamical properties of such black holes have been already studied both in asymptotically flat [3] and curved [4] spacetimes. Unfortunately, the temperature and entropy which have been derived are not sufficient to describe the detailed evaporation spectrum through the emission of Hawking radiation: the exact coupling between the black hole and the quantum fields, i.e. the greybody factors, must be accurately computed. To date, the greybody factors have been obtained for D -dimensional Schwarzschild [5, 6, 7] (for a detailed review, see [8]), Reissner-Nordstrom [9], Kerr [10, 11, 12, 13] and Schwarzschild-de-Sitter [14] black holes, for various types of emitted fields.

Furthermore, it has been recently pointed out that small black holes could be formed at next-generation colliders during transplanckian particle collisions [15] if the Planck scale is of order a TeV, as is the case in some scenarios postulating the existence of extra dimensions [16]. This idea has driven a considerable amount of interest in the framework of collider physics [17], as well as in cosmic-ray physics [18] as the same phenomenon could also occur during ultrahigh-energy neutrino interactions in the atmosphere of the earth. Most works consider those black holes as described by higher-dimensional generalizations of 4-dimensional line-elements that follow in the context of Einstein's linear theory of gravity. Studying the experimental consequences of the Gauss-Bonnet term, when included in the D -dimensional action, is a very challenging path strongly connected to experimentally probing quantum gravity. With arguments based solely on the dynamics of the temperature, it has been pointed out that for realistic values of the Gauss-Bonnet coupling constant and a low enough Planck scale, the LHC should be able to discriminate between a pure Einstein action and a second or-

der Lovelock action [19] upon the successful detection of the Hawking radiation emission spectrum from such a black hole.

To confirm this stimulating hypothesis it is nevertheless necessary to calculate the exact Gauss-Bonnet greybody factors values that have not been computed to date. The aforementioned work [19] used an approximate expression for the greybody factors to compute the emission spectrum from a Schwarzschild-Gauss-Bonnet black hole; this approximate expression ignored altogether its dependence on the energy and spin of the emitted particle as well as its dependence on the Gauss-Bonnet coupling constant itself. In this work, we calculate through numerical analysis the exact values of the Gauss-Bonnet greybody factors and the corresponding emission spectra for scalar, fermion and gauge boson fields restricted to live on our 4-dimensional brane. The spectrum for the emission of scalar fields in the bulk will also be studied, and the bulk-to-brane ratio will be accurately calculated. The dependence of the spectra on the Gauss-Bonnet coupling constant will be studied in detail, and footprints of its value would be looked for in both bulk and brane emission channels. As we will see, the implementation of the exact Gauss-Bonnet greybody factors will lead to modifications in the Hawking radiation emission spectra compared to the ones derived in the pure Schwarzschild case, and can also change the so-far derived results in the literature for the bulk-to-brane emission rates ratio.

In what follows, we will work in the context of the scenario with Large Extra Dimensions [16], and assume that the higher-dimensional spacetime is empty and thus flat. Also, the horizon value r_H of the produced black holes will be assumed to be much smaller than the (common) size R of the extra dimensions; under this assumption, the extra spacelike dimensions can be considered to be non-compact as the usual 3-dimensional ones. The energy of the emitted particle ω will be taken to be always much smaller than the black hole mass M_{BH} so that no significant back-reaction to the black hole background will take place after the emission of a particle. The frequency of the emitted particle must also be bounded from below, i.e. $\omega \geq 1/R$; this guarantees that the wavelength of the particle is much smaller than the size of the extra dimensions and the particle can therefore be considered as a genuinely higher-dimensional one. Although the upper limit on the frequency of the black hole will be always ensured in our analysis, for the sake of presenting complete spectra, the lower bound will be ignored and restored at the end of our analysis.

Section 2 of this paper sets the general framework for our analysis. The absorption cross-sections, i.e. the greybody factors, are then numerically computed for particles on the brane and in the bulk in sections 3 and 4, respectively. Section 5 presents the final Hawking radiation emission spectra for both brane and bulk channels, and the bulk-to-brane emission rates ratios is explicitly given. We discuss our results and summarise our conclusions in section 6. The numerical values of the greybody factors produced in this analysis, that might be useful for experimental searches, can be downloaded from the URL given in [20].

2 General Framework

A higher-dimensional, neutral, static, spherically-symmetric black hole within the framework of a curvature-squared, Gauss-Bonnet gravity is described by the following line element, first derived in [21] and then extended to a different topology in [4]:

$$ds^2 = h(r) dt^2 - \frac{dr^2}{h(r)} - r^2 d_{D-2}^2; \quad (1)$$

where d_{D-2}^2 is the line element over a unitary $(D-2)$ -dimensional sphere and

$$h(r) = k + \frac{r^2}{2 \frac{\Gamma(D-3)\Gamma(D-4)}{\Gamma(D-2)} \Gamma(D-4)} \left[1 + \frac{64 \frac{\Gamma(D-3)\Gamma(D-4)GM_{BH}}{\Gamma(D-2)} r^{D-1}}{\Gamma(D-2)} \right] \quad (2)$$

is the metric function. In the above, $\Gamma(D-2)$ corresponds to the total $(D-2)$ -dimensional solid angle. In [21], it was shown that a Schwarzschild-like spacetime within Gauss-Bonnet gravity exhibits two branches corresponding to the signs entering the metric function. The (+)-sign branch describes a Schwarzschild black hole with a negative ADM mass embedded in an Anti-de Sitter Universe whereas the (-)-sign branch corresponds to an asymptotically flat Schwarzschild black hole with a positive ADM mass. In addition, Gauss-Bonnet gravity leads to a ghost graviton, when expanded around an AdS background, yielding the (+)-sign branch to be unstable. The author of Ref. [4] extended the solution of [21] to different topologies for the black hole's event horizon: for $k = 1$, the event horizon is elliptic whereas it becomes flat for $k = 0$ and hyperbolic for $k = -1$ [22]. In this work, we restrict our analysis to the (-)-sign branch with an elliptic topology for the event horizon, as it corresponds to the usual Schwarzschild black hole solution. The (+) branch will be hereafter ignored and the k parameter will be set equal to $+1$.

As in higher-dimensional general relativity, Schwarzschild-Gauss-Bonnet black holes present one event horizon located at r_H and defined as the solution of the algebraic equation $h(r) = 0$. The thermodynamical properties of those black holes have been extensively studied in [4]. For non-rotating, neutral black holes, the thermodynamics is described by three quantities, all parametrized by the horizon radius: the mass M_{BH}

$$M_{BH} = \frac{\Gamma(D-2) \frac{D-1}{2} r_H^{D-3}}{8G \frac{D-1}{2}} \left[1 + \frac{\Gamma(D-3)\Gamma(D-4)}{r_H^2} \right]; \quad (3)$$

where Γ stands for the Euler Gamma function, the temperature T_{BH} given by the surface gravity evaluated at the event horizon radius,

$$T_{BH} = \frac{\Gamma(D-3) [r_H^2 + \Gamma(D-5)\Gamma(D-4)]}{4 r_H [r_H^2 + 2 \Gamma(D-4)\Gamma(D-3)]}; \quad (4)$$

and the entropy S_{BH} , defined by

$$S_{\text{BH}} = \int \frac{dM_{\text{BH}}}{T_{\text{BH}}} : \quad (5)$$

The Hawking radiation emission process by the black hole given in Eq. (1) takes place in the higher-dimensional space-time with a spectrum given by the generalization of the four-dimensional one obtained in [23] :

$$\frac{dN_s(\omega)}{dt} = \sum_j \frac{\gamma_{j;s}(\omega)}{\exp(\omega/T_{\text{BH}})} \frac{d^{D-1}k}{(2\pi)^{2s} (2\omega)^{D-1}} : \quad (6)$$

In the above equation, j stands for the total angular momentum quantum number and s for the spin of the particle. In this work, we will focus on massless particles for which $|j| = |s|$; in this case, the expression for the flux is greatly simplified as the phase space term reduces to an integral over the energy of the emitted particle

$$\frac{d^2N_s(\omega)}{dt d\omega} = \sum_j \frac{\gamma_{j;s}(\omega) \omega^{D-2}}{\exp(\omega/T_{\text{BH}})} \frac{d^{D-2}}{(2\pi)^{D-1}} : \quad (7)$$

The function $\gamma_{j;s}(\omega)$, usually called "greybody factor" or alternatively "absorption/emission cross section", when accurately taken into account, makes the resulting radiation spectrum more complex than the usual blackbody law. This additional factor arises because of the non-vanishing probability for the emitted particles to be reflected on the gravitational potential barrier and re-absorbed by the black hole. The cross section is computed within a full quantum mechanical framework to determine first the tunnelling transmission probability $\mathcal{T}_{j;s}$ in the aforementioned Schwarzschild-Gauss-Bonnet background. The cross section for a given angular momentum quantum number is then deduced from the generalization of the optical theorem [24] :

$$\gamma_{j;s}(\omega) = \frac{2^{D-4} (D-3)^{-2} ((D-3)-2)!}{(D-4)! \omega^{D-2}} \frac{(2j+D-3)(j+D-4)!}{j!} \mathcal{T}_{j;s}^2 : \quad (8)$$

As it is clear from the above, the Hawking radiation emission spectrum is defined by two quantities, the black hole temperature and the particle's greybody factor. From Eq. (4), we may see that the temperature has an explicit dependence on both the Gauss-Bonnet coupling constant and the dimensionality of spacetime. As we will see, the greybody factor depends, too, upon the underlying gravitational theory and thus encodes valuable information on both of these parameters; as expected, it also depends on properties of the emitted particle such as its energy and spin. This elaborate dependence of the greybody factor on a number of fundamental parameters of the theory is the main motivation for performing the exact calculation of its value and of the corresponding black hole radiation spectrum within the framework of a D -dimensional Gauss-Bonnet gravity.

3 Radiation on the brane

3.1 General equation for particles on the brane

Particles confined on the brane propagate into a background whose geometry is induced by the bulk curvature. This induced geometry on the 4-dimensional brane is simply given by fixing the values of the extra azimuthal angular coordinates, $\theta_i = \pi/2$, and leads to the projection of the D -dimensional metric on the 4-dimensional slice that describes our world. The projected metric has the form :

$$ds^2 = h(r)dt^2 - \frac{dr^2}{h(r)} - r^2 d\Omega^2 + \sin^2 \theta d\phi^2 ; \quad (9)$$

where the metric function $h(r)$ remains the same as in the higher-dimensional line-element given in Eq. (1). Consequently, the profile of the curvature along the three non-compact spatial dimensions contains a footprint of the bulk curvature.

The equations of motion describing the behavior of particles with spin restricted to our 4-dimensional brane are deduced by using the Newman-Penrose formalism [25, 26]. Under the assumption of minimal coupling to gravity, these equations can be combined into one master equation for particles with spin $s = 0; 1/2; 1$. In [8] (see also [10]), this master equation was derived for particles confined on a brane embedded in a D -dimensional Kerr black hole background. In the limit of zero black hole angular momentum, the Kerr metric reduces to the Schwarzschild one, and the induced background on the brane assumes the form given in Eq. (9). Using the following factorized ansatz for the propagating field:

$$\psi_s(t; r; \theta; \phi) = e^{i\omega t} e^{im\phi} P_s(r) Y_{s,j}^m(\theta) \quad (10)$$

where $\rho = hr^2$ and j is the total angular momentum quantum number, the radial part of the master equation of motion is found to have the form :

$$\frac{d}{dr} \left(\frac{1}{h} \frac{dP_s}{dr} \right) + \left(\frac{\omega^2}{h} + 2is\omega r \right) P_s - \frac{j(j+1)r^2 h^0}{h} P_s = 0 \quad (11)$$

In the above, $\tilde{\omega} = j(j+1) - s(s-1)$ is derived from the master angular equation satisfied by the spin-weighted spherical harmonics $Y_{s,j}^m$ [27].

The aforementioned master equation has been successfully used to derive the Hawking radiation emission spectrum on the brane for scalar, fermion and gauge boson fields by a D -dimensional Schwarzschild black hole [5, 6, 7], and for scalar fields by a D -dimensional Schwarzschild-de Sitter black hole [14]. Recently, its complete form, that includes a non-vanishing black hole angular momentum, was used to study the emission of scalar fields on the brane by a D -dimensional Kerr black hole [11, 13]. In our case, since the line-element of a D -dimensional Schwarzschild-Gauss-Bonnet black hole has a Schwarzschild-like form, Eq. (11)

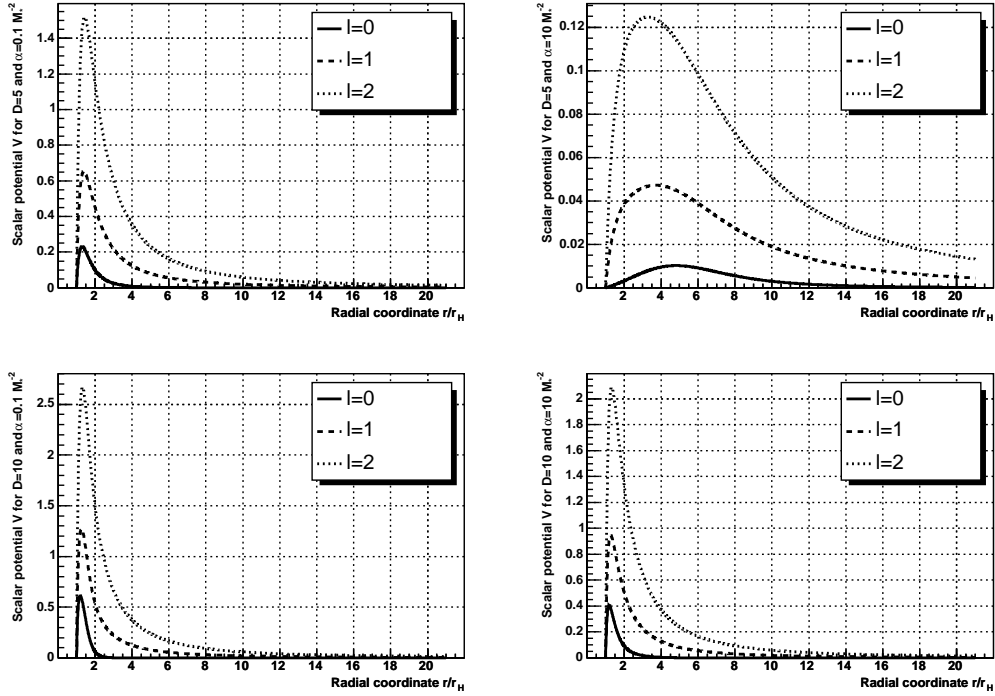


Figure 1: Gravitational potential seen by scalar particles propagating in the background of an induced Schwarzschild-Gauss-Bonnet black hole. Upper Panels: The number of dimensions is fixed at 5 and the Gauss-Bonnet coupling constant at $0.1 M^{-2}$ on the left and at $10 M^{-2}$ on the right. Lower Panels: The number of dimensions is fixed at 10 and the Gauss-Bonnet coupling constant at $0.1 M^{-2}$ on the left and at $10 M^{-2}$ on the right.

can be consistently used to study the emission of scalar¹, fermion and gauge boson fields emitted by such a black hole on the brane.

Writing the master equation (11) for scalar particles in an alternative form allows to validate our approach to be followed in the next section. By using the tortoise coordinate r^* , defined by $h(r)dr^* = dr$, and redefining the unknown radial function by $U(r) = rP_0(r)$, the scalar equation takes a Shrodinger-like form :

$$\frac{d^2U}{dr^{*2}} + h(r) \left[\frac{l(l+1)}{r^2} + \frac{h^0(r)}{r} \right] U = \omega^2 U ; \quad (12)$$

where l is the orbital angular momentum. From the above equation, the gravitational potential seen by scalar particles can be easily read, and it is depicted in Fig. 1 for various values of the fundamental parameters of the theory. This poten-

¹The equation of motion for a scalar field propagating in a D dimensional Schwarzschild-Gauss-Bonnet black hole background was recently studied in [28] to obtain the evolution of the scalar field in time and its quasinormal modes.

tial, for Schwarzschild-Gauss-Bonnet black holes, tends to zero both at the black hole's event horizon and at spatial infinity, due to the vanishing of the metric function in the first case and the asymptotic flatness of space-time in the second. The corresponding near-horizon and far-field asymptotic states can be therefore defined in terms of plane waves, a result that allows the use of the optical theorem for the computation of the absorption cross-section. Figure 1 clearly shows that the height of the potential barrier is increasing for modes with increasingly larger angular momentum number, and a similar effect arises as the dimensionality of space-time increases, too. On the other hand, the height of the barrier is considerably lowered as the value of the Gauss-Bonnet coupling increases, with the effect being more significant for low values of D .

3.2 Numerical results for the absorption cross-section

Equation (11) has been attacked analytically in the literature, and results have been produced for the absorption cross-section (see for instance Refs. [5, 6, 14]) under the assumption of low-energy emitted particles. As the gravitational background, however, becomes more complicated, our ability to solve this equation analytically is greatly reduced. Moreover, the need to produce exact results, free from any approximations and valid throughout the energy regime, dictates the use of numerical analysis. The intricate shape of the metric function (2) in this particular case makes Eq. (11) impossible to solve analytically. Therefore, in this work, the calculation of the absorption cross section is performed numerically, for particles with spin $s = 0; 1=2$ and 1 .

The numerical integration of Eq. (11) starts from the black hole horizon, where appropriate boundary conditions are applied, and extends to spatial infinity. In order to deal with finite numbers and avoid divergences at the horizon, the numerical integration starts at $r_{\text{ini}} = r_H + \epsilon$ instead of r_H , where ϵ is small enough to induce a negligible only error. As mentioned before, the asymptotic solution near the horizon is of a plane-wave form. In order to simplify the numerical analysis, the P_s function and its derivative are fixed, at r_{ini} , to the following values :

$$P_s(r_{\text{ini}}) = 1 \tag{13}$$

$$\frac{dP_s}{dr} = \frac{i!}{h(r_{\text{ini}})}; \tag{14}$$

which ensure that the no-outgoing modes boundary condition is satisfied, and fix the flux at the black hole event horizon to $\mathcal{F}_s^2 = 1$.

The solution of the master equation is then propagated from the event horizon until a high enough value of the radial coordinate r , to be considered as spatial infinity. At this asymptotic regime, the wave function must be described by

spherical waves [5]:

$$P_s(r) \sim B_1 \frac{e^{i\omega r}}{r^{1-2s}} + B_2 \frac{e^{i\omega r}}{r}; \quad (15)$$

where B_1 is the amplitude of the ingoing modes and B_2 the amplitude of the outgoing modes. The numerical results are then compared to the above asymptotic solution, and a fit is performed in order to extract the amplitudes B_1 and B_2 . As it is obvious from the above asymptotic solution, for scalar particles with $s = 0$, the solution of the master equation at infinity contains both ingoing and outgoing modes. For particles with non-vanishing spin though, the complete solution follows by solving a set of two equations: one for the upper component $s = +|j|$ which is mainly composed of ingoing modes, and one for the lower component $s = -|j|$, which is mainly composed of outgoing modes [30]. The absorption probability can be found through the ratio of the incoming flux at infinity over the one at the horizon, therefore only the solution for the ingoing modes is necessary for our study, and thus only the upper component of Eq. (11) is solved. The absorption cross-section is then easily computed in terms of the absorption probability, through Eq. (8) evaluated for $D = 4$ to account for brane emission:

$$\sigma_j(\omega) = \frac{(2j+1)}{4} \frac{\mathcal{A}_j^2}{\omega^2}; \quad (16)$$

To obtain the total absorption cross-section, all the angular momentum contributions have to be summed. Fortunately, as it is shown in Fig. 1, the gravitational potential barrier increases with j , and the high angular momentum contributions are strongly suppressed. The sum is therefore performed until rank $j = m$ such that the error due to higher momentum contributions becomes irrelevant.

In the case of particles with non-vanishing spin, another difficulty arises due to the very small value of the outgoing modes in the upper component of the wave function. As these modes are extremely small at the event horizon, a tiny error in the numerical solution can easily be mixed with an outgoing solution and can consequently contaminate the ingoing one. As a result, the numerical integration is not stable as it strongly depends on the boundary conditions. This contamination does not arise for fermions, but it becomes significant for gauge boson fields, and the absorption cross-section cannot be robustly computed by integrating Eq. (11). A solution to overcome this problem has been proposed in [7] and consists in solving the equation of motion for a new unknown radial wave function $F(y)$, defined as $P_1 = yF(y)e^{i\omega r^*}$, with $y = r - r_H$. In terms of these new variables, the wave equation for gauge boson fields becomes:

$$hy^2 \frac{d^2 F}{dy^2} + 2y(h^2 - \omega^2) \frac{dF}{dy} - j(j+1)F = 0 \quad (17)$$

with the following boundary conditions having replaced the ones in Eq. (14): $F(1) = 1$ and $dF/dy(1) = ij(j+1)/2r_H$.

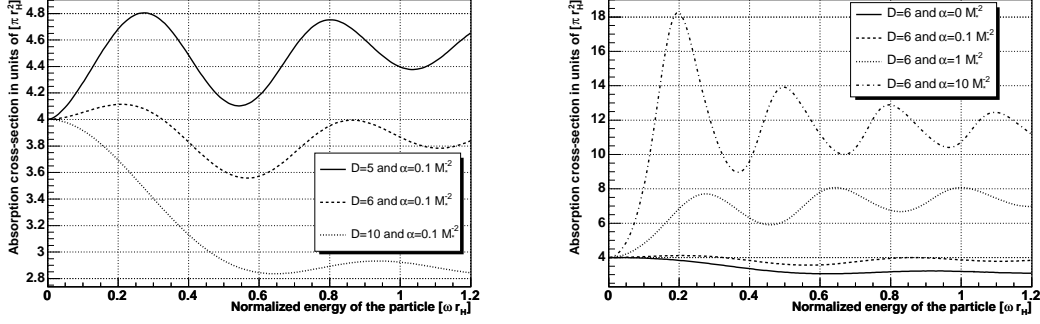


Figure 2: Absorption cross-section for scalar fields on the brane for Schwarzschild-Gauss-Bonnet black holes as a function of the energy of the particle ωr_H . Left Panel: the Gauss-Bonnet coupling constant is fixed at $0.1 M^{-2}$ and the number of dimensions D at $\{5; 6; 10\}$. Right Panel: the Gauss-Bonnet coupling constant takes the values $\{0; 0.1; 1; 10\} M^{-2}$ and the number of dimensions is fixed at 6.

3.2.1 Absorption cross-section for scalars

The absorption probability is defined as the ratio of the ingoing flux F at infinity over the one at the event horizon. For scalar particles, the flux is given by the radial part of the conserved current $J = 2hr^2 \text{Im}(\dot{\phi} \partial_r \phi^*)$, which leads to $F = 2hr^2 \text{Im} \left(\frac{P_0}{r^2} \frac{d}{dr} r^2 P_0^* \right)$. The absorption probability is found to have the form

$$\mathcal{A}_{jj} = r_H^2 \frac{1}{B_1} = 1 \frac{B_2}{B_1}; \quad (18)$$

where, in the middle part, we have used the fact that the ongoing flux at the black hole horizon has been fixed to 1 by the boundary condition (14). The last part of the above equation offers an alternative but equivalent way of calculating \mathcal{A}_{jj} through the reflection probability given in terms of the amplitudes of the ingoing and outgoing modes at infinity.

Figure 2 shows the numerical results we have obtained for the absorption cross-section in units of r_H^2 as a function of the dimensionless parameter ωr_H . The two panels depict results for: a fixed value of the Gauss-Bonnet coupling constant and variable D , the first one, and a fixed value of D and variable α , the second. In both panels, when $\omega r_H \rightarrow 0$, the absorption cross-section tends to a non-vanishing value ($4 r_H^2$), which does not depend on the number of dimensions or on the value of the Gauss-Bonnet coupling constant. This behaviour follows the same pattern seen in other cases of asymptotically-flat spherically-symmetric black hole backgrounds [5, 7, 29] emitting scalar radiation: in the low-energy regime, the absorption cross-section reduces to the area of the black hole horizon – for brane emission, this is simply $4 r_H^2$.

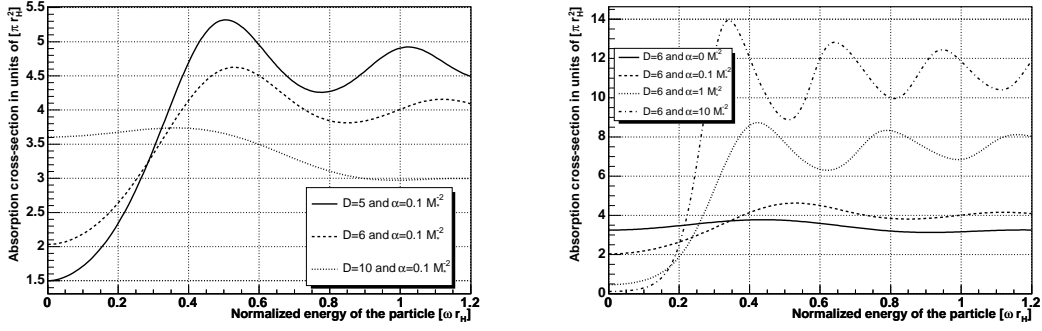


Figure 3: Absorption cross-section for fermion fields on the brane for Schwarzschild-Gauss-Bonnet black holes as a function of the energy of the particle ωr_H . Left Panel : the Gauss-Bonnet coupling constant is fixed at $0.1 M^2$ and the number of dimensions D at $\{5, 6, 10\}$. Right Panel : the Gauss-Bonnet coupling constant takes the values $\{0, 0.1, 1, 10\} M^2$ and D is fixed at 6.

On the contrary, the behaviour of the cross-section in all other energy regimes strongly depends on both the number of dimensions and on the Gauss-Bonnet coupling constant : as for the case of Schwarzschild and Schwarzschild-de Sitter black holes, an increase in the number of dimensions leads to a decrease of the absorption cross-section [7, 14]. On the other hand, an increase of the Gauss-Bonnet coupling constant leads to an increase of the absorption cross-section. Both of these results could be inferred from the behavior of the gravitational potential, that was derived in section 3.1, with respect to D and α : the potential increases when D increases whereas it decreases when α increases. The oscillatory behavior of the absorption cross-section, that follows as modes with higher angular momentum numbers gradually come into dominance, is also affected by the presence of the Gauss-Bonnet term : the frequency of the oscillations increases with the Gauss-Bonnet coupling constant.

3.2.2 Absorption cross-section for fermions

For fermion fields, the ingoing flux is defined as the radial component of the conserved current $J^A = 2 \epsilon_{AB} \frac{A}{1=2} \frac{B}{1=2}$ evaluated over a two dimensional sphere (see [30] for an explicit calculation). As in the case of scalar fields, this flux has to be calculated both at the black hole's event horizon and at spatial infinity in order to find \mathcal{A}_j^2 . Once this is done, the absorption probability for a mode with an angular momentum j is found to be

$$\mathcal{A}_j^2 = \frac{1}{B_1}^2 : \quad (19)$$

Unlike the scalar case, we can not use the outgoing flux to determine the absorption coefficient because we have only considered the upper component of the fermion fields.

Figure 3 displays the numerical evaluation of the absorption cross-section for fermion particles on the brane. The high-energy limit of this cross-section is equal to the one for scalar particles and behaves in the same way with respect to the number of dimensions and to the Gauss-Bonnet coupling constant: the high-energy limit increases with the Gauss-Bonnet coupling constant whereas it decreases with the number of dimensions. When $r_H \rightarrow 0$, the absorption cross-section tends to a non-vanishing value which behaves similarly to the Schwarzschild case with respect to the number of dimensions: an increase in the value of D leads to an increase of the low-energy asymptotic value of the absorption cross-section (we refer the reader to [5, 7] for an exhaustive discussion). The Gauss-Bonnet term leaves also a footprint on the asymptotic value of the cross-section when $r_H \rightarrow 0$: this asymptotic value decreases when the Gauss-Bonnet coupling increases. As in the high energy limit, the Gauss-Bonnet coupling constant changes the absorption cross-section in an opposite way than the number of dimensions does.

3.2.3 Absorption cross-section for gauge bosons

For gauge boson fields, the ingoing flux is derived from the trace of the energy-momentum tensor $T_{AB} = 2 g_{AB} \partial^A \phi \partial^B \phi$ evaluated, as for fermions, over a two dimensional sphere. An explicit calculation of the flux at the black hole's event horizon and at spatial infinity leads to the absorption coefficient [30, 6]:

$$\mathcal{A}_{JJ} = \frac{1}{r_H^2} \frac{1}{B_1} : \quad (20)$$

Despite a few quantitative differences, we may clearly see from Fig. 4 that the absorption cross-section in the case of gauge bosons exhibits a similar behavior to fermions with respect to the number of dimensions and to the Gauss-Bonnet coupling constant. The high-energy regime asymptotic values are again suppressed with the number of dimensions and enhanced with the value of the Gauss-Bonnet coupling constant. The main difference occurs in the asymptotic regime of low energy: the absorption cross-section tends to zero when $r_H \rightarrow 0$, a behavior exhibited also in the pure Schwarzschild case [6]. Although the asymptotic value of the absorption cross-section vanishes in this regime, the statement that an increase in the Gauss-Bonnet coupling constant leads to a decrease of the cross-section at low energy is still valid as it falls down to zero more rapidly for higher values of α . On the contrary, the cross-section approaches zero slower for higher values of the number of dimensions.

From the previous results, we can summarize the effect of the Gauss-Bonnet term on the absorption cross-section as follows: for scalar particles, an increase of

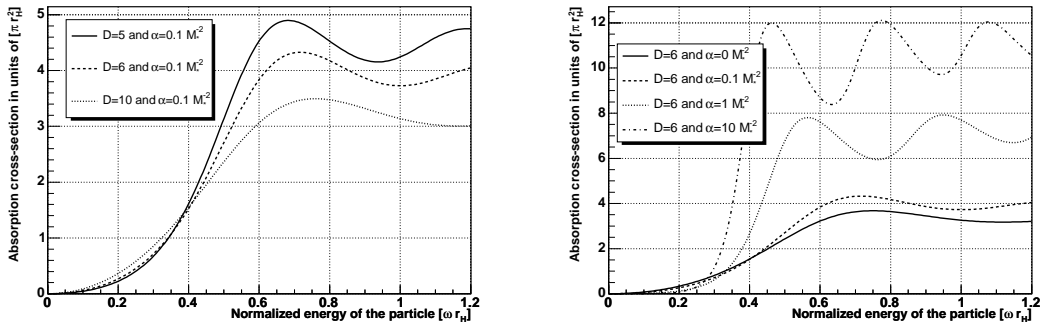


Figure 4: Absorption cross-section for gauge bosons on the brane for Schwarzschild-Gauss-Bonnet black holes as a function of the energy of the particle ωr_H . Left Panel : the Gauss-Bonnet coupling constant is fixed at $0.1 M^2$ and the number of dimensions D at $\{5;6;10\}$. Right Panel : the Gauss-Bonnet coupling constant takes the values $\{0;0.1;1;10\} M^2$ and D is fixed at 6.

the Gauss-Bonnet coupling constant leads to an increase of the absorption cross-section over the whole energy spectrum. For particles with non-vanishing spin, an increase of the Gauss-Bonnet coupling constant leads to an increase of the absorption cross-section in the high-energy regime whereas it decreases it in the low-energy regime. Finally, the effect of the number of dimensions is the same as for Schwarzschild black holes and affects the cross-section in exactly the opposite way that the Gauss-Bonnet coupling constant does. As a similar behavior is also exhibited by the temperature of the black hole in terms of its dependence on α and D , it becomes increasingly more interesting to compute the thermal emission rate to decide on the prevailing factor (temperature or absorption cross-section) that shapes the radiation spectrum for this particular black-hole background.

3.3 Semi-analytical results for the high energy limit

As it is known, and was numerically checked in the previous subsections, in the high-energy regime, the greybody factor assumes its geometrical optics limit value, which is independent of the spin of the emitted particle. This limiting value has been successfully used in both 4-dimensional and higher-dimensional black-hole backgrounds [7, 14] to describe the greybody factor of the corresponding black hole. This technique makes use of the geometry around the emitting (or absorbing) body and the same method can be applied for a Schwarzschild-Gauss-Bonnet projected black hole: for a massless particle in a circular orbit around a black hole, described by a line-element of the form (9), its equation of motion, $p_p = 0$, can be written in the form

$$\frac{1}{r} \frac{dr}{d\tau}^2 = \frac{1}{b^2} - \frac{h(r)}{r^2}; \quad (21)$$

$\sigma_g = (r_H^2)$	$= 0$	$= 0.1$	$= 1$	$= 10$
D = 5	4.00	4.59	9.46	51.2
D = 6	3.07	3.91	7.64	11.4
D = 7	2.60	3.53	5.70	6.62
D = 8	2.31	3.24	4.53	4.88
D = 9	2.12	3.00	3.82	3.98
D = 10	1.98	2.80	3.34	3.43
D = 11	1.87	2.63	3.00	3.06

Table 1: High-energy limits of the greybody factor on the brane in units of r_H^2 .

where b is the ratio of the angular momentum of the particle over its linear momentum. The classically accessible regime is defined by the relation $b < m$ in $(r = r_H)$. The above result is valid for all spherically-symmetric Schwarzschild-like line-elements of the form (9) with the structure of the particular gravitational background entering the above relation through the metric function $h(r)$. In order to compute the critical value of the parameter b , we must first minimize the function $r = r_H$; this takes place at $r = r_c$, where r_c is defined through the relation

$$1 + \frac{64}{(D-2)(D-3)(D-4)} \frac{GM_{BH}}{r_c^{D-1}} = \frac{8}{(D-2)(D-3)} \frac{GM_{BH}}{r_c^3} : \quad (22)$$

Then, b_c is found by evaluating the function $r = r_H(r)$ at the value $r = r_c$. The corresponding area, $\sigma_g = b_c^2$, defines the absorptive area of the black hole at high energies and, thus, its greybody factor (being a constant, the emitting body is characterized at high energies by a blackbody radiation spectrum). Its exact expression comes out to be

$$\sigma_g = \frac{r_c^2}{1 + \frac{r_c^2}{2(D-3)(D-4)}} \frac{r_c^2}{1 + \frac{64}{(D-2)(D-3)} \frac{GM_{BH}}{r_c^{D-1}}} : \quad (23)$$

For $D = 4$ and $\sigma = 0$, $r_c = 3r_H$ and the above expression reduces to the four-dimensional one, $\sigma_g = 27 r_H^2 = 4$. For arbitrary values, however, of D and σ , Eq. (22) can not be solved in a closed form, and the value of r_c can be found only numerically in terms of D , σ , and, through Eq. (3), r_H . In Table 1, we display the values of the greybody factor under the geometric optics approximation, in units of r_H^2 , for various values of D and σ , and for $r_H = 1$. It can easily be checked that these results are in excellent agreement with the high-energy behavior of the numerically computed greybody factors presented in the previous subsections.

4 Radiation in the bulk

4.1 Equation for scalar particles in the bulk

Although all Standard Model (SM) particles are confined to our 4-dimensional brane, scalar particles which are neutral with respect to the SM charges are allowed to propagate in the bulk. As a consequence, black holes can radiate spin-0 particles out of the brane and this radiation, although invisible to us, contributes to the total mass-loss rate. In order to make accurate estimates of the amount of energy radiated by the black hole on the brane, it is therefore necessary to determine the absorption cross-section and eventually the energy emission rate for those particles, too.

The generalization of the Klein-Gordon equation to a D -dimensional curved space-time is given by $\square \psi = 0$, where ψ runs over the D dimensions. In the spherically symmetric case, the following ansatz is used :

$$\psi(t; r; \omega_i; l) = e^{i\omega t} P(r) Y^m(\omega_i; l) \quad (24)$$

where $Y^m(\omega_i; l)$ stands for the D -dimensional generalization of the spherical harmonics [31]. With this ansatz, the radial part of the Klein-Gordon equation, satisfied by the unknown function $P(r)$, takes the form :

$$\frac{h(r)}{r^{D-2}} \frac{d}{dr} \left(r^{D-2} h(r) \frac{dP}{dr} \right) + \omega^2 \frac{h(r)}{r^2} (l^2 + D - 3) P = 0: \quad (25)$$

Apart from an implicit dependence upon the number of dimensions through the metric function h , the bulk equation exhibits also an explicit dependence through the contribution of the $D - 2$ compact dimensions entering the kinetic term and through the eigenvalues associated to the D -dimensional spherical harmonics. These contributions modify the exact form of the centrifugal potential, however, its general behaviour remains the same vanishing both at the black hole horizon and spatial infinity. Therefore the solution of the above equation at these two asymptotic regimes will again be given in terms of plane waves.

Although the basis for the Hawking radiation process in the bulk is the same as for emission on the brane, both analytical and numerical studies of Eq. (25) have shown that varying the number of dimensions have different quantitative consequences on the bulk greybody factor and emission rate, for Schwarzschild [5, 7] and Schwarzschild-de Sitter black holes [14]. As in those studies, we expect the number of dimensions as well as the Gauss-Bonnet coupling constant to strongly modify the value of the absorption cross-section for scalar particles in the case of a Schwarzschild-Gauss-Bonnet black hole, too.

4.2 Numerical results for the absorption cross-section

We numerically evaluate the absorption cross-section for emission in the bulk by following the same method as in the case of brane emission: Eq. (25) is numerically integrated starting from the vicinity of the black hole's event horizon, at $r_{\text{ini}} = r_H + \epsilon$, where the boundary conditions (14) have been again applied, and propagating the solution until spatial infinity. The analytical asymptotic solutions at spatial infinity, given by [5]

$$P_0(r) = B_1 \frac{e^{i\omega r}}{r^{D-2}} + B_2 \frac{e^{-i\omega r}}{r^{D-2}}; \quad (26)$$

are then fitted on the numerical results and the amplitude of both ingoing and outgoing modes are extracted from the fit parameters. Once again, the absorption probability $|\mathcal{A}_{\omega j}|^2$ is linked to these amplitudes via Eq. (18), and the absorption cross-section is obtained using the D -dimensional generalization of the optical theorem given in Eq. (8).

Our results are shown in Fig. 5 where the absorption cross-section is expressed in units of the black hole's area A_{D-2} , i.e. the area of a $(D-2)$ -dimensional sphere with radius r_H

$$A_{D-2} = r_H^{D-2} (2\pi)^{(D-3)/2} \frac{D-1}{2}; \quad (27)$$

These plots exhibit the same qualitative behavior as for the brane emission case: the absorption cross-section tends to a non-vanishing value when $\omega r_H \rightarrow 0$, increases with the Gauss-Bonnet coupling constant while it decreases for higher D values. From a quantitative point of view, the number of dimensions leaves a clear footprint on the asymptotic value in the low energy regime as $\sim A_{D-2}$, which only depends on the size of the black hole and the number of dimensions, a behavior similar to the one found in the D -dimensional Schwarzschild black hole case [7]. The effect of the Gauss-Bonnet coupling constant, on the other hand, is greatly enhanced when compared to what happens in the case of brane emission. The significant enhancement of the bulk absorption cross-section, as the Gauss-Bonnet coupling constant increases, will play a significant role in the determination of the bulk-to-brane emission rates ratio to be computed in Section 5.3. Another novel characteristic, that arises in the case of a Schwarzschild-Gauss-Bonnet black hole, is the fact that the bulk absorption cross-section is enhanced by the number of extra dimensions from the intermediate energy regime and onwards – in the case of a pure D -dimensional Schwarzschild black hole, the absorption cross-section in the bulk was heavily suppressed with the number of dimensions in the low- and intermediate-energy regimes allowing only for a small enhancement in the high-energy part of the spectrum [7, 8, 14].

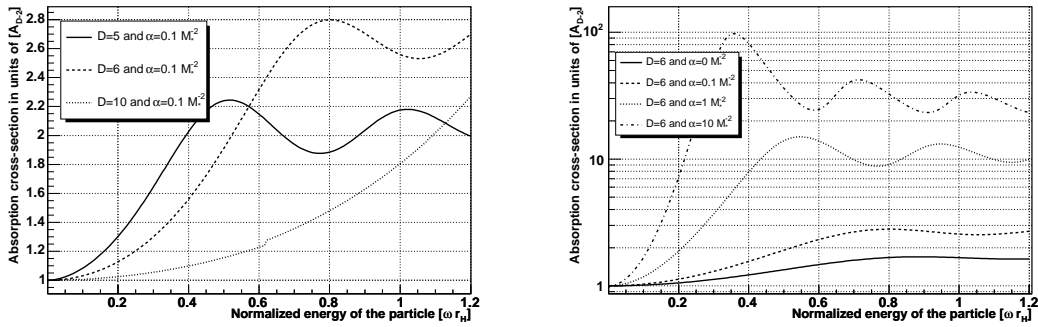


Figure 5: Absorption cross-section for scalar fields in the bulk for Schwarzschild-Gauss-Bonnet black holes as a function of the energy of the particle ωr_H . Left Panel: the Gauss-Bonnet coupling constant is fixed at $0.1 M^2$ and the number of dimensions D at $5; 6; 10$. Right Panel: the Gauss-Bonnet coupling constant takes the values $0; 0.1; 1; 10 M^2$ and the number of dimensions is fixed at 6.

4.3 Semi-analytical results for the high energy limit

For emission in the bulk, the high-energy limit of the absorption cross-section is again given by the geometric optics approximation. The classically accessible regime for D -dimensional spacetimes of the form described in Eq. (1) is again given by $b < m$ in ($r = r_h$) [32], with the minimum radial proximity b_c obtained as in Section 3.3. What nevertheless changes, in the case of propagation in a higher-dimensional black-hole background, is the expression of the absorptive area of the black hole as a function of the critical radius b_c : as it was pointed out in Ref. [7], when carefully computed, this area comes out to be

$$A_p = \frac{2}{(D-2)} \frac{(D-4)^2}{[(D-2)^2]} b_c^{D-2} : \quad (28)$$

This area stands for the absorption cross-section σ_g , or greybody factor, for particle emission in the bulk at high energies.

In Table 2, we give some indicative values of the greybody factor, in units of the area of the D -dimensional horizon A_{D-2} , for emission of scalar fields in the bulk at high-energies, for particular values of D and α , and for $r_H = 1$. Once again, these asymptotic values are in good agreement with the numerical results obtained in the $\omega r_H \rightarrow 1$ limit, and reveal the enhancement of the absorption cross-section in this energy regime, in terms of both the Gauss-Bonnet coupling constant and the dimensionality of spacetime.

$\gamma_{\text{D}} = A_{\text{D}-2}$	$\gamma = 0$	$\gamma = 0.1$	$\gamma = 1$	$\gamma = 10$
D = 5	1.70	2.09	6.19	77.7
D = 6	1.77	2.87	11.0	24.5
D = 7	1.85	3.97	13.2	19.1
D = 8	1.93	5.31	14.6	18.1
D = 9	2.01	6.81	15.8	18.3
D = 10	2.08	8.40	17.0	19.0
D = 11	2.16	10.0	18.3	19.9

Table 2: High-energy limits of the greybody factor in the bulk in units of $A_{\text{D}-2}$.

5 Particle emission spectrum

In this section, the Hawking radiation spectrum emitted by a Schwarzschild-Gauss-Bonnet black hole is computed using the exact numerical results derived in the previous sections for the absorption cross-section. The spectrum is evaluated for scalar particles, emitted on the brane and in the bulk, and for fermion and gauge boson particles emitted on the brane. We also compare the number of scalar particles emitted on the brane and in the bulk as a function of the Gauss-Bonnet coupling constant, number of dimensions and mass of the evaporating black hole. It was pointed in Ref. [14] that the calculation of the temperature of a Schwarzschild-de Sitter black hole is not simply given by the surface gravity as it is not possible to place an observer at spatial infinity. Such a modification in the temperature computation is a direct consequence of the intrinsic curvature of space-time. In the present case, the space-time is asymptotically flat and we can safely use the surface gravity to compute the Schwarzschild-Gauss-Bonnet black hole temperature given by equation (4). Consequently, the radiation spectra derived hereafter are relative to an observer infinitely far from the black hole.

Up to this point, all thermodynamical quantities of the Schwarzschild-Gauss-Bonnet black hole, as well as the greybody factors, were conveniently expressed in terms of the event horizon radius r_{H} . Comparing the values of these quantities, as the parameters D and γ varied while r_{H} remained fixed, was indeed an easy task. It also allowed for a direct comparison of our results to those derived previously in the literature under the same normalization. However, from an observational point of view, the horizon radius is not a convenient parameter to measure (and thus to fix), as different values of D and γ correspond to black holes with different masses. Therefore, for observational convenience, in what follows, the various radiation spectra will be derived and compared at fixed black hole masses.

5.1 Radiation spectrum on the brane

For massless particles emitted on the brane, the flux spectrum, i.e. the number of particles emitted per unit time and unit frequency by the black hole, is given by Eq. (7) evaluated for $D = 4$:

$$\frac{d^2 N_s}{dt d\omega} = \frac{1}{(2\pi)^3} \frac{4\pi \omega^3 (s!)^2}{e^{\omega/T_H} (1\omega)^s}; \quad (29)$$

where s is the spin of the emitted field. Figures 6, 7 and 8 depict flux spectra for scalars, fermions and gauge bosons, respectively, emitted by a higher-dimensional Schwarzschild-Gauss-Bonnet black hole. As the dependence of these spectra on the number of dimensions is similar to the one obtained in the case of a higher-dimensional Schwarzschild black hole, that has been exhaustively studied in the literature already [5, 6, 7], here we choose to focus on the effect of the Gauss-Bonnet coupling constant instead. We thus fix the number of dimensions at $D = 6$, and assign to α the values $\{0; 0.1; 1; 10\} \text{gM}^{-2}$. In the case of scalar fields, shown in Fig. 6, the particle emission spectrum was also derived for four different values of the black hole mass, i.e. for $\{10; 100; 1000; 10000\} \text{gM}$. The spectra for fermions and gauge bosons are shown only for the two extreme mass values as their behavior is qualitatively identical to the one seen in the scalar case.

From these plots, we may clearly see the non-monotonic effect that the Gauss-Bonnet coupling constant has on the number of emitted particles. We can also clearly see a strong dependence of the spectrum on the mass of the evaporating black hole. A number of competing factors contribute to the non-monotonic behaviour in terms of ω displayed in Fig. 6: although the greybody factor for scalar fields is greatly enhanced in units of the horizon area, the horizon radius itself shrinks under an increase in the value of the Gauss-Bonnet coupling, when we keep the mass of the black hole fixed; in addition, the temperature of the black hole as a function of α is also non-monotonic (a simple numerical analysis shows that it initially decreases with α but, after a turning point is reached, it starts increasing again). All the above factors tend to compensate each other, with the outcome of this process greatly depending on the black hole mass value: for light black holes, the reduction of the horizon radius, as α increases, is a significant one which, in conjunction with the decreasing temperature, leads to the suppression of the number of particles emitted – only after the turning point of the temperature is reached does the spectrum show some enhancement. For heavier black holes, the effect on the value of the horizon radius, as well as the decline of the temperature with α , tends to become less and less important; the increase of the absorption cross-section then prevails over all other factors, thus leading to an enhancement of the radiation spectrum as the value of α increases.

Similar arguments hold for the case of the emission on the brane of fermions and gauge bosons. In both cases, for low-mass black holes, the decrease of the

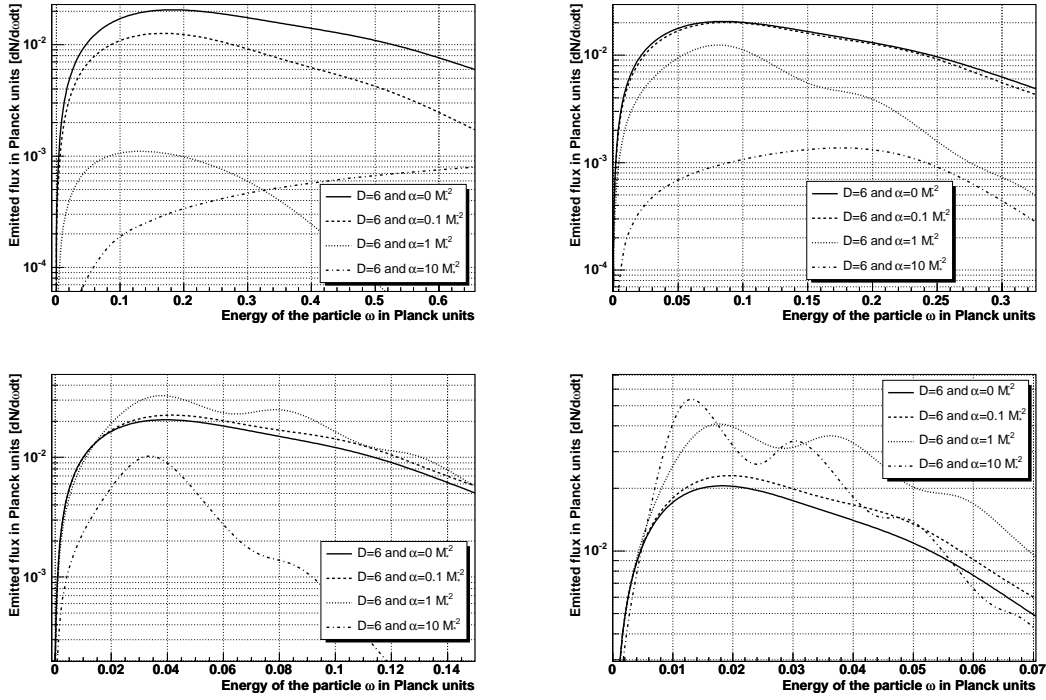


Figure 6: Flux spectrum for scalar fields emitted on the brane by a Schwarzschild-Gauss-Bonnet black hole as a function of the energy ω . The Gauss-Bonnet coupling constant takes the values $\alpha = 0; 0.1; 1; 10 g M^{-2}$ and the number of dimensions is fixed at 6. The mass of the black hole is taken equal to $M_{BH} = 10 M$ (upper left), $M_{BH} = 100 M$ (upper right), $M_{BH} = 1000 M$ (lower left) and $M_{BH} = 10000 M$ (lower right).

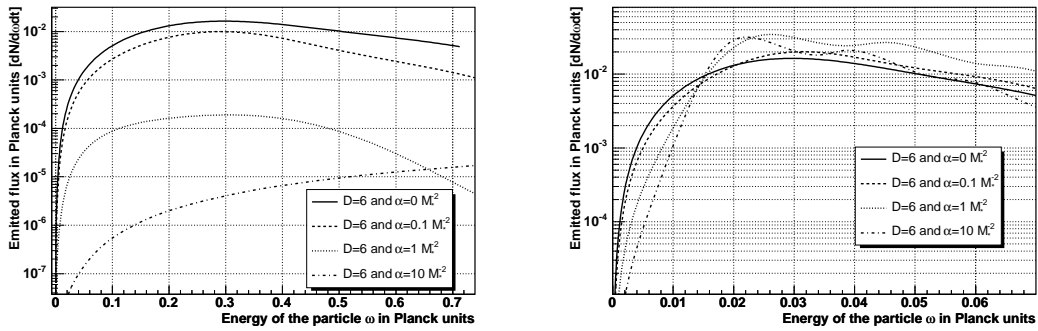


Figure 7: Flux spectrum for fermion fields emitted on the brane by a Schwarzschild-Gauss-Bonnet black hole as a function of the energy ω . The Gauss-Bonnet coupling constant takes the values $\alpha = 0; 0.1; 1; 10 g M^{-2}$ and the number of dimensions is fixed at 6. The mass of the black hole is $M_{BH} = 10 M$ on the left panel, and $M_{BH} = 10000 M$ on the right panel.

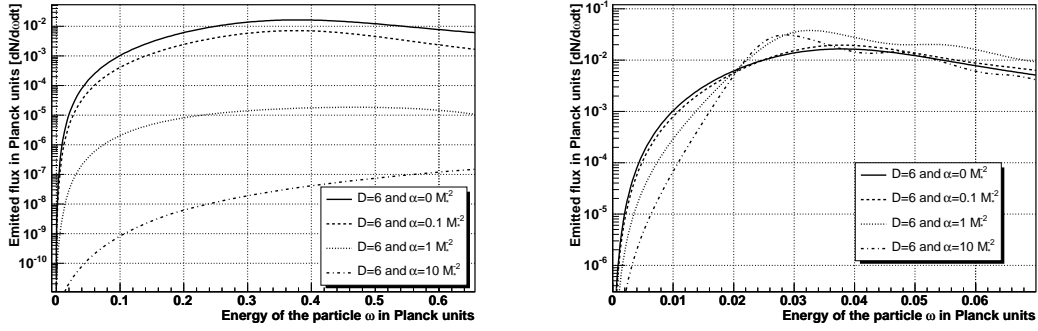


Figure 8: Flux spectrum of gauge bosons emitted on the brane by a Schwarzschild-Gauss-Bonnet black hole as a function of the energy ω . The Gauss-Bonnet coupling constant takes the values $\alpha = 0, 0.1, 1, 10 \text{ gM}^{-2}$ and the number of dimensions is fixed at 6. The mass of the black hole is $M_{\text{BH}} = 10M$ on the left panel, and $M_{\text{BH}} = 10000M$ on the right panel.

horizon radius and of the temperature leads to a suppression of the number of particles emitted, even in the intermediate and high-energy regime where the greybody factor was greatly enhanced as a function of ω ; only for large values of the Gauss-Bonnet coupling constant does the spectrum shows signs of enhancement as a reaction again of the change in the temperature behavior. For black holes with larger masses, the enhancement of the greybody factor with ω , found for the intermediate and high-energy regime, prevails again and eventually leads to a small enhancement in the number of particles emitted. This enhancement is slightly smaller than the one found in the case of the scalar fields as a result of the radically different behaviour of the greybody factor for different fields at the low-energy regime: while the enhancement, in terms of ω , seen in this energy regime gives a boost in the spectrum of scalar fields, its suppression for fermion and gauge bosons restricts the enhancement of the flux spectrum at higher energy regimes.

Let us finally note here that the non-monotonic behavior of the temperature of a Schwarzschild-Gauss-Bonnet black hole as a function of the Gauss-Bonnet coupling constant is clearly reflected on the value of the energy peaks in the particle spectra. For instance, the temperature of a 6 dimensional black hole with a mass of $10M$, is roughly equal to $T_{\text{H}} = 0.14; 0.11; 0.06; 0.5 \text{ gM}^{-1}$ for $\alpha = 0; 0.1; 1; 10 \text{ gM}^{-2}$. Focusing, for example, on the scalar particles spectrum emitted by a black hole with a mass of $10M$ (upper left panel of Fig. 6), we see that the peaks of the emission curves shift towards lower or higher energy values accordingly. Moreover, they correspond to energies lying in the range $1.4 \frac{1}{M}$ to $2 \frac{1}{M}$, depending on the exact value of α , which is in good agreement with the prediction for the location of the energy peak for a pure black-body spectrum at $1.6 \frac{1}{M}$.

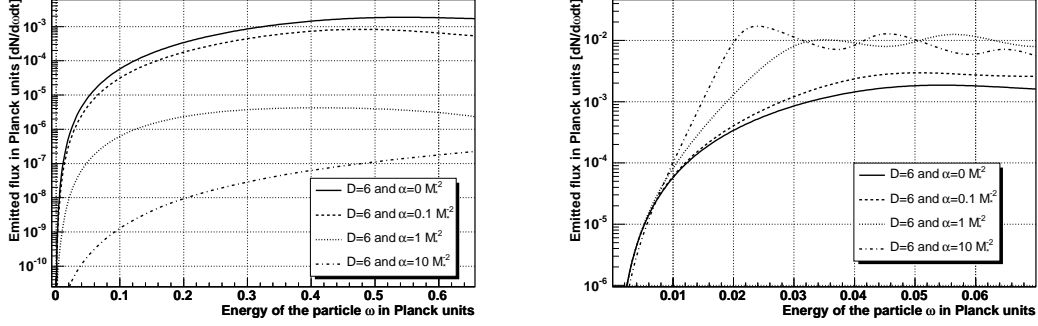


Figure 9: Flux spectrum for scalar fields emitted in the bulk by a Schwarzschild-Gauss-Bonnet black hole as a function of the energy ω . The Gauss-Bonnet coupling constant takes the values $\alpha = 0, 0.1, 1, 10 \text{ gM}^{-2}$ and the number of dimensions is fixed at 6. The mass of the black hole is $M_{\text{BH}} = 10M_{\text{pl}}$ on the left panel, and $M_{\text{BH}} = 10000M_{\text{pl}}$ on the right panel.

5.2 Radiation spectrum in the bulk

For massless particles emitted in the bulk, the Hawking radiation spectrum is given by :

$$\frac{d^2N}{dt d^D} = \frac{1}{(2\pi)^{D-1}} \frac{D-2}{e^{1/T_H}} \frac{(\omega)^{D-2}}{1} ; \quad (30)$$

where the spin index is omitted as only scalar fields can propagate into the bulk (gravitons are not considered in this work). By using our numerical results for the bulk absorption cross-section, derived in section 4.2, we may now proceed to derive the particle emission spectrum for emission in the bulk of scalar fields. The absorption cross-section will be expressed in units of the D -dimensional black hole area $A_{D-2} = (D-2) r_H^D$, but, as in the previous subsection, we choose the mass of the black hole as its characteristic parameter that remains fixed.

The flux spectra for scalar particles emitted in the bulk by a 6-dimensional black hole, with a mass of $10M_{\text{pl}}$ and $10000M_{\text{pl}}$, are shown in the two panels of Fig. 9, for a set of values of the Gauss-Bonnet coupling constant given by $\alpha = 0, 0.1, 1, 10 \text{ gM}^{-2}$. The spectra exhibit the same characteristics, in terms of their behavior as functions of the Gauss-Bonnet coupling constant, as in the case of scalar fields emitted on the brane. When the mass of the black hole is only a few times above the Planck scale, the decrease in the horizon value and the temperature of the black hole, when α increases, eventually leads to the suppression of the flux spectrum, despite the enhancement of the absorption cross-section over the whole energy regime in units of the black hole's area. For significantly heavier black holes though, the magnitude of this enhancement overcomes the decrease in the area and temperature of the black hole, leading to a significant increase in the number of particles emitted, especially for high values of α .

5.3 Bulk-to-brane ratio

The bulk-to-brane relative emission is of great importance for experimental investigations: particles emitted in the bulk cannot be detected, and the corresponding energy will be permanently lost. It was shown in Refs. [7, 14] that this ratio remains lower than one for D -dimensional Schwarzschild and D -dimensional Schwarzschild-de Sitter black holes. Such results clearly favour the scenario of the experimental detection of small black holes through the emission of Hawking radiation since most of their energy will be spent on the emission of brane-localised particles. However, as it was mentioned in Section 4.2, for Schwarzschild-Gauss-Bonnet black holes, the effect of the Gauss-Bonnet coupling constant on the absorption cross-section is more important for particles emitted in the bulk than for particles emitted on the brane. Therefore, we can not exclude the possibility that such black holes can decay mainly in the bulk channels instead of the brane channels. We expect this to happen especially in the high-energy regime, where the cross-section is more significantly enhanced, and for heavy black holes, for which the effect of the greybody factor dominates the spectrum.

In Fig. 10, we present the outcome of our attempt to check this possibility numerically by using our results for the bulk and brane particle emission rates for scalar fields. The four panels of this figure show the bulk-to-brane ratio for a 6-dimensional black hole with a mass equal to $M_{\text{BH}} = f10;100;1000;10000gM_{\text{pl}}$, respectively, and for different values of the Gauss-Bonnet coupling constant. As we see, in almost all cases, the relative emission rate remains lower than one, although it asymptotically approaches this value in the high-energy regime. As expected, this ratio exceeds unity only in the case of a black hole with mass of $10000M_{\text{pl}}$ and only in the high-energy part of the spectrum. Therefore, it seems highly possible that, as we increase further the value of the black hole mass, and for sufficiently high Gauss-Bonnet coupling constant, the bulk channel becomes increasingly more dominant, leading eventually to a significant loss of the black hole energy into the bulk.

An upper limit on the bulk-to-brane relative emission rate can be obtained by looking at the spectrum of black holes with fixed horizon radius instead of a fixed mass. Figure 11 (a) shows the spectrum of such a black hole. Since r_{H} is now kept fixed, the different curves shown in this figure for different values of the Gauss-Bonnet coupling constant correspond to black holes with different masses, according to Eq. (3). However, there is one case where all these curves would describe a black hole with the same mass, and that is the case of a black hole with an infinite mass (in that case, any change in α would produce a negligible change in the black hole mass). Therefore, Fig. 11 can be used to derive an upper limit for the bulk-to-brane ratio. As we may see, for high values of the Gauss-Bonnet coupling constant, the relative emission rate becomes indeed greater than one. This value is attained over the whole high-energy regime, and can therefore lead to a major loss of the black hole energy into the bulk.

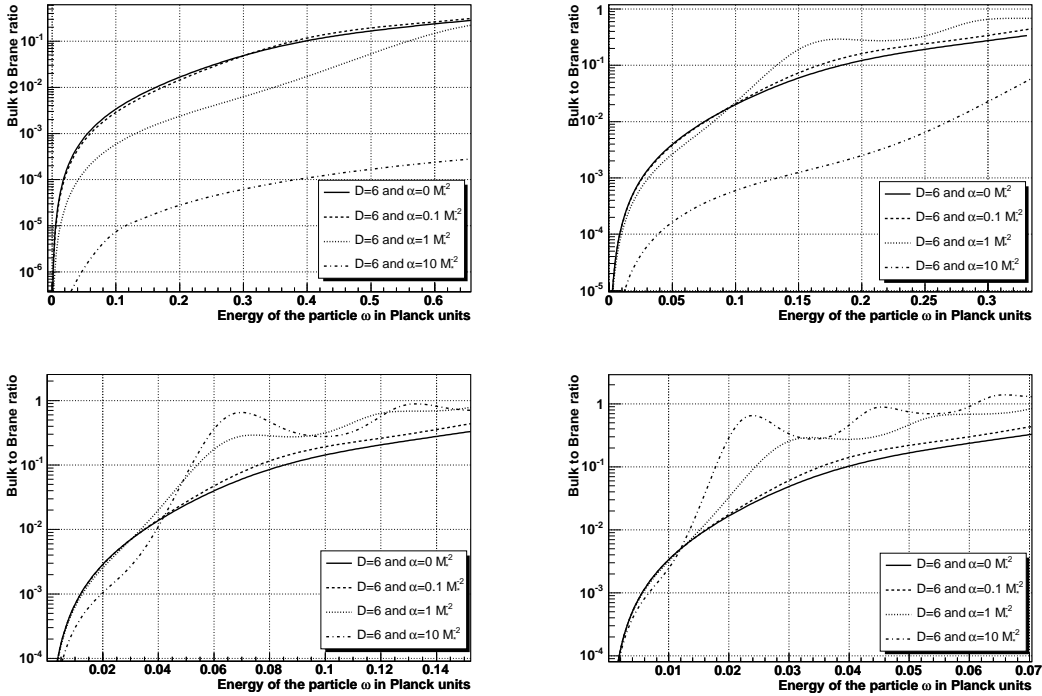


Figure 10: Bulk-to-brane relative emission rate as a function of the energy ω . The Gauss-Bonnet coupling constant takes the values $\alpha=0;0.1;1;10gM^{-2}$ and the number of dimensions is fixed at 6. The mass of the black hole is taken to be $M_{BH} = 10M$ (upper left), $M_{BH} = 100M$ (upper right), $M_{BH} = 1000M$ (lower left) and $M_{BH} = 10000M$ (lower right).

(or, even the decay of the black hole mainly through the bulk channel) via the emission of particles with $\omega > 1=r_H$. We should, however, note here that such a scenario is not experimentally favored as it requires very high values for the Gauss-Bonnet coupling constant and black hole masses above the values that could be reached by the next-generation colliders. The behavior of the bulk-to-brane relative emission rate for an intermediate value of the Gauss-Bonnet coupling constant, i.e. $\alpha=0.1 M^{-2}$, is shown in Fig. 11 (b) as a function of the number of dimensions: as in the case of a pure D dimensional Schwarzschild black hole [7] it remains lower than one and decreases for higher dimensional black holes.

6 Conclusions

Looking for gravitational effects beyond general relativity is a major experimental challenge. Lovelock gravity (especially its curvature-squared Gauss-Bonnet term) is an interesting way of extending the Einstein-Hilbert action in a string-inspired

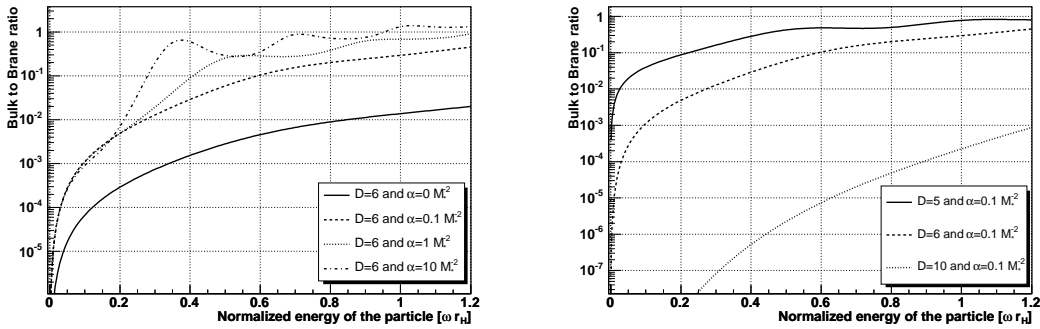


Figure 11: Bulk-to-brane relative emission rate as a function of the unidimensional parameter ωr_H for 6 dimensional black holes with a given size. Left Panel: the Gauss-Bonnet coupling constant is taken at $\{0; 0.1; 1; 10\} \text{g M}^{-2}$ and the number of dimensions is fixed at $D = 6$. Right Panel: the Gauss-Bonnet coupling constant is fixed at 0.1 M^{-2} and the number of dimensions is taken at $\{5; 6; 10\}$.

approach. As was shown in [19], Schwarzschild-Gauss-Bonnet black holes, that could also be formed at colliders, would allow an accurate investigation of the associated coupling constant. This paper goes beyond the approximation made in [19] for the expression of the Hawking radiation emission rate of these black holes, and presents the complete, exact particle spectrum by including the missing material, i.e. the greybody factors.

More analytically, in this paper, we have investigated the decay of a D dimensional Schwarzschild-Gauss-Bonnet black hole via the emission of Hawking radiation. For this purpose, we have computed the exact expressions for the greybody factors for scalar, fermion and gauge boson fields emitted on the brane as well as for scalar fields emitted in the bulk by using numerical analysis. These results have revealed that the absorption cross-sections depend strongly not only on the energy and spin of the emitted particle and the dimensionality of spacetime but also on the value of the Gauss-Bonnet coupling constant. Interestingly enough, it turns out that the effect of this coupling constant on the absorption cross-section is exactly the opposite of the one of the dimensionality of spacetime: this quantity is enhanced over the whole energy regime for scalar fields (emitted both on the brane and in the bulk) while, for fermions and gauge fields, it is enhanced in the intermediate- and high-energy regime and suppressed in the low-energy regime.

With these results at hand, we proceeded to evaluate the particle emission spectra for all types of particles. At this point, we switched from the convenient assumption of a black hole with a fixed horizon radius to the phenomenologically realistic one of a black hole with a fixed mass $\{$ that allowed us to reveal and emphasize the importance of the mass of the black hole on the behavior of the radiation spectra with respect to the Gauss-Bonnet coupling constant. Our

results have shown that, for light black holes, an increase in the value of the Gauss-Bonnet coupling constant leads to the suppression of the number of particles emitted by the black hole per unit time and unit frequency, for all types of particles. This is the result of the ensuing decrease of the black hole's area and temperature dominating over any enhancement exhibited by the greybody factor. However, for heavy black holes, it is the enhancement of the greybody factor that overcomes the small, in this case, decrease of the black hole's area and temperature, thus leading to a spectrum that is also predominantly enhanced with the Gauss-Bonnet coupling constant.

The bulk-to-brane relative emission rates have also been computed for the emission of scalar fields that are allowed to propagate both on and off the brane. They were shown to be also black-hole-mass and coupling-constant-dependent. Whereas, for small or zero Gauss-Bonnet coupling constant, this ratio remains always smaller than unity (thus favoring the detection of mini-black holes through their decay mainly on the brane where our detectors are located) (this situation may easily change for heavy black holes and sufficiently high Gauss-Bonnet coupling constant). Nevertheless, any significant effect of this type would demand black hole masses beyond the order of $10000 M_{\text{pl}}$ and a Gauss-Bonnet coupling constant of order $10 M_{\text{pl}}^2$. Therefore, for black holes with masses attainable at next-generation colliders, their decay will take place mainly through brane channels, even if quadratic curvature terms are taken into account in the theory.

To conclude, let us note that the above results have been derived under the assumption that the extra spacelike dimensions can be considered as non-compact. This assumption might be violated if the black hole radius becomes comparable to or larger than the size of the extra dimensions. Depending on the number of dimensions, the latter varies in the range of a few femis to a few millimeters in order to obtain a Planck scale of order a TeV without being in contradiction with any experimental observations. As black holes produced at next-generation colliders will not be heavier than $10 M_{\text{pl}}$, their sizes will remain much lower than a femi, and our calculations can therefore be safely used to compute the decay of higher-dimensional Schwarzschild-Gauss-Bonnet black holes. Finally, our results apply for particles with wavelengths lower than the size of the extra dimensions, which then defines a lower limit on the particle's energy. Therefore, the interpretation of our results found for the very low-energy part of the derived spectra must be interpreted with care. This constraint however does not diminish the importance of our results or the possibility of detecting the presence of quadratic gravitational terms in the theory: the effect of the Gauss-Bonnet term becomes manifest in a clear way over the whole radiation spectrum, especially in the intermediate and high-energy regime.

Acknowledgments. The work of P.K. was funded by the UK PPARC Research Grant PPA/A/S/2002/00350.

References

- [1] D. Lovelock, *J. Math. Phys.* **12**, 498 (1971); *J. Math. Phys.* **13**, 874 (1972).
- [2] B. Zwiebach, *Phys. Lett. B* **156**, 315 (1985).
- [3] R. C. Myers and J. Z. Simon, *Phys. Rev. D* **38**, 2434 (1988).
- [4] R. G. Cai, *Phys. Rev. D* **65**, 084014 (2002) [[hep-th/0109133](#)]; *Phys. Rev. D* **69**, 104025 (2004) [[hep-th/0311020](#)].
- [5] P. Kanti and J. March-Russell, *Phys. Rev. D* **66**, 024023 (2002) [[hep-ph/0203223](#)].
- [6] P. Kanti and J. March-Russell, *Phys. Rev. D* **67**, 104019 (2003) [[hep-ph/0212199](#)].
- [7] C. M. Harris and P. Kanti, *JHEP* **0310**, 014 (2003) [[hep-ph/0309054](#)].
- [8] P. Kanti, *Int. J. Mod. Phys. A* **19**, 4899 (2004) [[hep-ph/0402168](#)].
- [9] E. Jung and D. K. Park, *Nucl. Phys. B* **717**, 272 (2005) [[hep-th/0502002](#)].
- [10] D. Ida, K. y. Oda and S. C. Park, *Phys. Rev. D* **67**, 064025 (2003) [Erratum – *ibid.* **D 69**, 049901 (2004)] [[hep-th/0212108](#)]; *Phys. Rev. D* **71**, 124039 (2005) [[hep-th/0503052](#)].
- [11] C. M. Harris and P. Kanti, [hep-th/0503010](#).
- [12] E. Jung and D. K. Park, [hep-th/0506204](#).
- [13] G. Du y, C. Harris, P. Kanti and E. W instanley, [hep-th/0507274](#).
- [14] P. Kanti, J. Grain and A. Barrau, *Phys. Rev. D* **71**, 104002 (2005) [[hep-th/0501148](#)].
- [15] T. Banks and W. Fischler, [hep-th/9906038](#);
D. M. Eardley and S. B. Giddings, *Phys. Rev. D* **66**, 044011 (2002) [[gr-qc/0201034](#)];
H. Yoshino and Y. Nambu, *Phys. Rev. D* **66**, 065004 (2002) [[gr-qc/0204060](#)];
Phys. Rev. D **67**, 024009 (2003) [[gr-qc/0209003](#)];
E. Kohprath and G. Veneziano, *JHEP* **0206**, 057 (2002) [[gr-qc/0203093](#)];
V. Cardoso, O. J. C. Dias and J. P. S. Lemos, *Phys. Rev. D* **67**, 064026 (2003) [[hep-th/0212168](#)];
E. Berti, M. Cavaglia and L. Gualtieri, *Phys. Rev. D* **69**, 124011 (2004) [[hep-th/0309203](#)];
L. A. Anchordoqui, J. L. Feng, H. Goldberg and A. D. Shapere, *Phys. Lett. B* **594** (2004) 363 [[hep-ph/0311365](#)];

- V. S. Rychkov, *Phys. Rev. D* 70, 044003 (2004) [[hep-ph/0401116](#)];
 S. B. Giddings and V. S. Rychkov, *Phys. Rev. D* 70, 104026 (2004) [[hep-th/0409131](#)];
 O. I. Vasilenko, [[hep-th/0305067](#)]; [[hep-th/0407092](#)];
 H. Yoshino and V. S. Rychkov, *Phys. Rev. D* 71 (2005) 104028 [[hep-th/0503171](#)];
 V. Cardoso, E. Berti and M. Cavaglia, *Class. Quant. Grav.* 22 (2005) L61 [[hep-ph/0505125](#)].
- [16] N. Arkani-Hamed, S. Dimopoulos and G. R. Dimand, *Phys. Lett. B* 429, 263 (1998) [[hep-ph/9803315](#)]; *Phys. Rev. D* 59, 086004 (1999) [[hep-ph/9807344](#)];
 I. Antoniadis, N. Arkani-Hamed, S. Dimopoulos and G. R. Dimand, *Phys. Lett. B* 436, 257 (1998) [[hep-ph/9804398](#)].
- [17] P. C. Argüres, S. Dimopoulos and J. March-Russell, *Phys. Lett. B* 441, 96 (1998) [[hep-th/9808138](#)];
 R. Emparan, G. T. Horowitz and R. C. Myers, *Phys. Rev. Lett.* 85, 499 (2000) [[hep-th/0003118](#)];
 S. B. Giddings and S. Thomas, *Phys. Rev. D* 65, 056010 (2002) [[hep-ph/0106219](#)];
 S. Dimopoulos and G. Landsberg, *Phys. Rev. Lett.* 87, 161602 (2001) [[hep-ph/0106295](#)];
 S. Dimopoulos and R. Emparan, *Phys. Lett. B* 526, 393 (2002) [[hep-ph/0108060](#)];
 S. Hossenfelder, S. Hofmann, M. Bleicher and H. Stöcker, *Phys. Rev. D* 66, 101502 (2002) [[hep-ph/0109085](#)];
 K. Cheung, *Phys. Rev. Lett.* 88, 221602 (2002) [[hep-ph/0110163](#)];
 R. Casadio and B. Harms, *Int. J. Mod. Phys. A* 17, 4635 (2002) [[hep-ph/0110255](#)];
 S. C. Park and H. S. Song, *J. Korean Phys. Soc.* 43, 30 (2003) [[hep-ph/0111069](#)];
 G. Landsberg, *Phys. Rev. Lett.* 88, 181801 (2002) [[hep-ph/0112061](#)];
 G. F. Giudice, R. Rattazzi and J. D. Wells, *Nucl. Phys. B* 630, 293 (2002) [[hep-ph/0112161](#)];
 E. J. Ahn, M. Cavaglia and A. V. Olinto, *Phys. Lett. B* 551, 1 (2003) [[hep-th/0201042](#)];
 T. G. Rizzo, *JHEP* 0202, 011 (2002) [[hep-ph/0201228](#)]; [[hep-ph/0412087](#)];
 A. V. Kotwal and C. Hays, *Phys. Rev. D* 66, 116005 (2002) [[hep-ph/0206055](#)];
 A. Chamblin and G. C. Nayak, *Phys. Rev. D* 66, 091901 (2002) [[hep-ph/0206060](#)];
 T. Han, G. D. Kribs and B. M. Kelso, *Phys. Rev. Lett.* 90, 031601 (2003) [[hep-ph/0207003](#)];
 I. Mocioiu, Y. Nara and I. Sarcevic, *Phys. Lett. B* 557, 87 (2003) [[hep-ph/0310073](#)];
 M. Cavaglia, S. Das and R. M. Aartens, *Class. Quant. Grav.* 20, L205 (2003)

- [hep-ph/0305223];
 C. M. Harris, P. Richardson and B. R. Webber, JHEP 0308, 033 (2003) [hep-ph/0307305];
 R. A. Konoplya, Phys. Rev. D 68, 124017 (2003) [hep-th/0309030]; Phys. Rev. D 71 (2005) 024038 [hep-th/0410057];
 V. Cardoso, J. P. S. Lemos and S. Yoshida, Phys. Rev. D 69 (2004) 044004 [gr-qc/0309112];
 M. Cavaglia and S. Das, Class. Quant. Grav. 21 (2004) 4511 [hep-th/0404050];
 D. Stojkovic, Phys. Rev. Lett. 94, 011603 (2005) [hep-ph/0409124];
 S. Hossenfelder, Mod. Phys. Lett. A 19, 2727 (2004) [hep-ph/0410122];
 C. M. Harris, M. J. Palmer, M. A. Parker, P. Richardson, A. Sabetfakhri and B. R. Webber, hep-ph/0411022;
 T. G. Rizzo, JHEP 0501 (2005) 028 [hep-ph/0412087]; JHEP 0506 (2005) 079 [hep-ph/0503163];
 J. L. Hewett, B. Lillie and T. G. Rizzo, hep-ph/0503178;
 L. Lonblad, M. Sjodahl and T. Akesson, hep-ph/0505181;
 B. Koch, M. Bleicher and S. Hossenfelder, hep-ph/0507138; hep-ph/0507140.
- [18] A. Goyal, A. Gupta and N. Mahajan, Phys. Rev. D 63, 043003 (2001) [hep-ph/0005030];
 J. L. Feng and A. D. Shapere, Phys. Rev. Lett. 88, 021303 (2002) [hep-ph/0109106];
 L. Anchordoqui and H. Goldberg, Phys. Rev. D 65, 047502 (2002) [hep-ph/0109242];
 R. Emparan, M. Masip and R. Rattazzi, Phys. Rev. D 65, 064023 (2002) [hep-ph/0109287];
 L. A. Anchordoqui, J. L. Feng, H. Goldberg and A. D. Shapere, Phys. Rev. D 65, 124027 (2002) [hep-ph/0112247]; Phys. Rev. D 68, 104025 (2003) [hep-ph/0307228];
 Y. Uehara, Prog. Theor. Phys. 107, 621 (2002) [hep-ph/0110382];
 J. Alvarez-Muniz, J. L. Feng, F. Halzen, T. Han and D. Hooper, Phys. Rev. D 65, 124015 (2002) [hep-ph/0202081];
 A. Ringwald and H. Tu, Phys. Lett. B 525, 135 (2002) [hep-ph/0111042];
 M. Kowalski, A. Ringwald and H. Tu, Phys. Lett. B 529, 1 (2002) [hep-ph/0111042];
 E. J. Ahn, M. Ave, M. Cavaglia and A. Volinto, Phys. Rev. D 68, 043004 (2003) [hep-ph/0306008];
 E. J. Ahn, M. Cavaglia and A. Volinto, Astropart. Phys. 22, 377 (2005) [hep-ph/0312249];
 T. Han and D. Hooper, New J. Phys. 6 (2004) 150 [hep-ph/0408348];
 A. Cafarella, C. Coriano and T. N. Tomaras, hep-ph/0410358;
 A. Barrau, C. Feron and J. Grain, astro-ph/0505436;
 L. Anchordoqui, T. Han, D. Hooper and S. Sarkar, hep-ph/0508312.

- [19] A. Barrau, J. Grain and S. O. Alexeyev, *Phys. Lett. B* 584, 114 (2004) [[hep-ph/0311238](#)].
- [20] <http://lpsc.in2p3.fr/ams/greybody/>
- [21] D. G. Boulware and S. Deser, *Phys. Rev. Lett.* 55, 2656 (1985).
- [22] D. Birmingham, *Class. Quant. Grav.* 16, 1197 (1999) [[hep-th/9808032](#)].
- [23] S. W. Hawking, *Commun. Math. Phys.* 43, 199 (1975).
- [24] S. S. Gubser, I. R. Klebanov and A. A. Tseytlin, *Nucl. Phys. B* 499, 217 (1997) [[hep-th/9703040](#)].
- [25] E. Newman and R. Penrose, *J. Math. Phys.* 3 (1962) 566.
- [26] S. Chandrasekhar, *The Mathematical Theory of Black Holes* (Oxford University Press, New York, 1983).
- [27] J. N. Goldberg, A. J. MacFarlane, E. T. Newman, F. Rohrlich and E. C. Sudarshan, *J. Math. Phys.* 8, 2155 (1967).
- [28] E. Abdalla, R. A. Konoplya and C. Molina, [hep-th/0507100](#).
- [29] E. L. Jung, S. H. Kim and D. K. Park, *Phys. Lett. B* 586, 390 (2004) [[hep-th/0311036](#)].
- [30] M. Cvetič and F. Larsen, *Phys. Rev. D* 57, 6297 (1998) [[hep-th/9712118](#)].
- [31] C. Müller, in *Lecture Notes in Mathematics: Spherical Harmonics* (Springer-Verlag, Berlin-Heidelberg, 1966).
- [32] R. Emparan, G. T. Horowitz and R. C. Myers, *Phys. Rev. Lett.* 85, 499 (2000) [[hep-th/0003118](#)].